Chiral logarithms in quenched m_π and f_π

Stephen R. Sharpe
Department of Physics, FM-15, University of Washington, Seattle, Washington 98195
(Received 16 January 1990)

A diagrammatic analysis predicts that, in the quenched approximation, there should be no chiral logarithms, at leading order, in m_π or f_π, for gauge groups SU($N \geq 3$). Morel has done an explicit calculation in the strong-gauge-coupling, large-dimension limit, and finds that there are such logarithms. I point out that Morel's calculation is of a quantity different from the quenched pion propagator. I show that if one calculates the correct quantity then there are no chiral logarithms. For SU(2), however, the diagrammatic analysis predicts that there are chiral logarithms in quenched m_π and f_π.

I. INTRODUCTION

This paper addresses the following question: Are there chiral logarithms in m_π and f_π when these quantities are calculated in the quenched approximation? An analysis of the quark diagrams which contribute implies that, for gauge groups SU($N \geq 3$), all diagrams giving rise to leading-order chiral logarithms contain internal quark loops. Since the quenched approximation removes all such loops, this analysis predicts that there should be no chiral logarithms, at leading order, in quenched m_π or f_π. This prediction is, however, in conflict with an explicit calculation by Morel.[1] He shows how to calculate chiral logarithms analytically, in both quenched and unquenched QCD, in the strong-coupling limit combined with a $1/d$ expansion. He finds that m_π and f_π, calculated in the quenched approximation, do contain chiral logarithms. Although far from the continuum limit, the strong-coupling theory should be amenable to the diagrammatic analysis, so this conflict cannot be an artifact of the approximations.

This paper resolves the conflict between Morel's explicit calculation and the diagrammatic analysis. It turns out that the explicit calculation is of the wrong quantity. Morel unwittingly includes contributions to the pion propagator, at one-loop order, which involve two disconnected quark lines. Examples are shown in Figs. 6(c) and 7(c) below. The quenched pion propagator does not include such disconnected diagrams. If one removes them, the chiral logarithms in m_π and f_π do cancel in the quenched approximation. Thus the diagrammatic analysis is correct.

Morel also calculates the chiral logarithms for the gauge group SU(2). This is a special case because there are Goldstone baryons (qq states) in addition to the usual Goldstone pions. Chiral logarithms are generated both by loops of pions [as for SU($N \geq 3$)], and by loops of Goldstone baryons. Some of the quark diagrams corresponding to loops of Goldstone baryons do survive in the quenched approximation. Examples are given in Fig. 8 below. Thus the diagrammatic analysis predicts that there should be chiral logarithms in quenched m_π and f_π if the gauge group is SU(2). Morel's calculation for SU(2) includes both the disconnected diagrams of Figs. 6(c) and 7(c) below, which should be discarded, and the baryon loop diagrams of Fig. 8 below, which should be kept. Thus while the numerical answer for the coefficient of the logarithm will change, Morel's qualitative conclusion remains valid for SU(2).

These results are important for two reasons. First, Morel's calculation was motivated by numerical results for the quantity $A = m_\pi^2/m_q$ obtained by Billoire and co-workers.[2] The calculation was done in the quenched approximation using the gauge group SU(2). In the chiral limit ($m_q \to 0$) one expects[3]

$$A = \frac{m_\pi^2}{m_q} = A_0 + A_1 m_\pi^2 + A_2 m_\pi^2 \ln \frac{m_\pi^2}{\Lambda^2} + O(m_\pi^4) . \quad (1)$$

Here Λ is an arbitrary scale which can be absorbed into A_1. For SU($N \geq 3$) the results of this paper imply that A_2 vanishes in the quenched approximation; i.e., $A_2^Q = 0$. For SU(2), however, a nonvanishing A_2 is predicted. It turns out that the numerical quenched results for A can only be fit well if an A_2-like term is included.[2] Morel's calculation provides theoretical justification for adding such a term. This qualitative explanation survives the reanalysis of this paper.

The verification of the diagrammatic analysis is also important because it can be applied to many quantities other than f_π and m_π. Of particular interest are kaon decay and mixing matrix elements. The analysis predicts that there are chiral logarithms in these quantities, even in the quenched approximation, and there is numerical evidence for such logarithms.[4]

The remainder of this paper explains the resolution of the disagreement between Morel's result and the diagrammatic analysis. Section II provides the necessary background and explains qualitatively why Morel's calculation includes diagrams which are not part of the quenched approximation. Section III shows by explicit calculation that, if these extra diagrams are removed, there are no chiral logarithms in m_π, for SU($N \geq 3$). The calculation uses a simple generalization of Morel's

methods. The technical device is the use of two species of fermions, which allows one to calculate nonsinglet propagators in which there can be no disconnected diagrams. Finally, in a brief section I discuss how the results change if the gauge group is SU(2).

In order to keep technical details to a minimum I frequently refer to equations in Morel's paper. These are labeled as I.1, I.2, etc. For detailed justification of the methods used to carry out the strong-coupling and large-d expansions, readers are referred to Ref. 5.

II. DIAGRAMMATIC ANALYSIS

We are interested in leading-order chiral logarithms in m_π. Such logarithms result from the long-distance part of the loops in the diagram shown in Fig. 1(a). The coefficient of the logarithm is calculable because chiral symmetry relates the pion four-point coupling to f_π and m_π. This is true both for continuum QCD and the lattice theory with staggered fermions, as follows from chiral Ward identities.[6] The only difference between the two theories is the numerical value of the coefficient A_2 in Eq. (1). This depends on the number of flavors of pions that can appear in the loop. The actual numerical values will not be important here.

One can also draw the quark diagrams which correspond to the chiral loops of Fig. 1(a). One example is shown in Fig. 1(b). The crucial point is that in all such quark diagrams there must be at least one internal quark loop. This can also be seen in a continuum chiral-Lagrangian calculation by following the flavor indices.[7] The only diagrams not involving internal quark loops are those of Fig. 1(c). For these, however, the four-pion vertex involves gluon exchange. By following flavor indices in a chiral-Lagrangian calculation, it can be seen that this vertex is absent at lowest order. Thus Fig. 1(c) gives only nonleading chiral logarithms, terms of relative size $m_\pi^4 \ln m_\pi^2$.

This analysis implies that, in the quenched approximation, in which internal quark loops are not included, there will be no chiral logarithms in m_π^2 at leading order, i.e., $A_2^Q = 0$. Similar arguments imply that there are no chiral logarithms at leading order in quenched f_π. These arguments depend in no obvious way on whether the theory is on the lattice or in the continuum, nor on the values of the coupling g or the dimension d. Thus they are in contradiction with Morel's results, which are obtained for $g=\infty$ and keeping terms of order $1/d$ in a large-d expansion.

To explain how this disagreement is resolved I must give some details of the $g\to\infty$, large-d theory. Morel calculates using staggered fermions, which have a remnant axial U(1) symmetry on the lattice. This symmetry is broken dynamically, so that there is a single Goldstone boson, which I will call the pion. It is the chiral logarithms in the mass of this boson that are at issue.

First let me discuss the full, unquenched theory. This has the partition function

$$Z_{\rm UQ} = \int [dU\, d\chi\, d\bar{\chi}]\, e^{-S_{\rm KS} - S_{\rm gauge}}\ , \tag{2}$$

$$S_{\rm KS} = -\bar{\chi}\left[\not{D}_U + m_q + \left[\frac{d}{2}\right]^{1/2} j \right]\chi\ , \tag{3}$$

where $\not{D}$ has the standard definition given in I.2, and I have followed Morel's normalization for the source j. The pion propagator is given by

$$G^\pi_{xy} = \langle \bar{\chi}\chi(x)\bar{\chi}\chi(y)\rangle_C = \frac{2}{d}\frac{\delta^2 \ln Z_{UQ}}{\delta j(x)\delta j(y)}\bigg|_{j=0}\ . \tag{4}$$

The gauge field U belongs to SU(N); its action is $S_{\rm gauge}$. In the strong-coupling limit the gauge action vanishes, so that the gauge fields have no dynamics. The integration over the gauge fields can be done analytically as an expansion in $1/d$ (Ref. 5). The result is a theory of mesons in which the quark and antiquark always occupy the same lattice site. The condensate $\sum_x \langle \bar{\chi}\chi(x)\rangle / V$, where V is the volume, has a nonzero value, which breaks the U(1)$_A$ symmetry. Corresponding to this, there is a Goldstone-boson pole in G^π at a momentum close to $q=(\pi,\pi,\pi,\pi)$. There are also poles at other momenta, corresponding to meson states such as the ρ, all of which have masses $O(1/a)$, a being the lattice spacing.

The $g\to\infty$, $d\to\infty$ limit is clearly far from the continuum. Staggered fermions represent four continuum flavors, so that one would expect 15 Goldstone bosons rather than one, together with a whole spectrum of light ρ's and other mesons. The sole advantage of the limit is that one can perform nonperturbative analytic calculations in a theory with a dynamically broken axial symmetry. This allows one to test general hypotheses. In particular, as realized by Morel, it is possible to compare quenched and unquenched calculations of chiral logarithms.

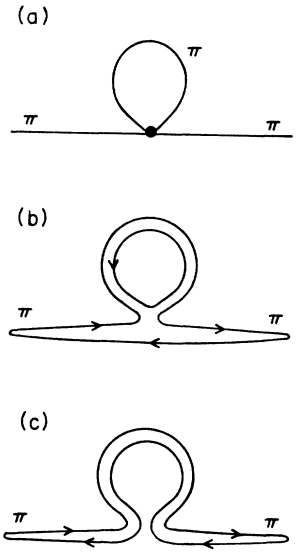

FIG. 1. Diagrams giving rise to chiral logarithms in f_π. (a) Meson diagram (the lines represent pions); (b) quark line diagram contributing at leading order; (c) quark diagram contributing only at nonleading order. In (b) and (c) it is implied that the diagram can be dressed with any number of gluons.

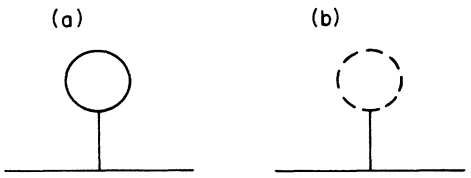

FIG. 2. Diagrams giving rise to chiral logarithms in m_π. Solid lines are bosons, dashed lines are fermions, as explained in the text.

Morel defines the quenched theory by adding a complex scalar ghost

$$Z_Q = \int [dU\, d\chi\, d\bar{\chi}\, d\phi\, d\phi^\dagger] \exp[-S_{\rm KS} - \phi^\dagger(\not{D}_U + \mu)\phi] \ . \tag{5}$$

In Green's functions the determinant from the $\chi,\bar{\chi}$ integrals is exactly canceled by that from the $\phi,\phi^\dagger$ integrals, as long as $\mu = m_q$. Since it is the determinant which contains the internal quark loops, Z_Q is exactly the partition function simulated in quenched calculations. The scalar fields have the wrong metric, so that the quenched theory is not unitary, as is well known. In the strong-coupling limit, the theory now has four light particles, all of which become massless in the limit $m_q = \mu \to 0$. There are two bosons created by $\bar{\chi}\chi$ and $\phi^\dagger\phi$, and two fermions created by $\bar{\chi}\phi, \phi^\dagger\chi$. The corresponding poles in all four propagators lie near the momentum $q = (\pi,\pi,\pi,\pi)$. There are also heavy bosons and fermions with masses of $O(1/a)$. In all these states, the particle and antiparticle propagate together without separating.

These particles interact with each other at local vertices of all orders. Thus there are loop corrections to the propagator. Each extra loop brings in a factor of $1/d$ (Ref. 5), so that the leading correction to the pion propagator comes from the one-loop diagrams shown in Figs. 2–4. The solid lines represent the bosonic states created by $\bar{\chi}\chi$, while the dashed lines represent the fermionic states (created by $\bar{\chi}\phi$). The diagrams with internal fermions, i.e., Figs. 2(b), 3(b), and 4(b), are absent in the full theory.

Figures 2(a), 3(a), and 4(a) are the strong-coupling equivalent of Fig. 1(a). It is important to realize that, even at strong coupling, there are only vertices involving even numbers of Goldstone pions. Thus, since the external lines in all diagrams are pions, the tadpole stem in Fig. 2(a) must be one of the heavy states. Similarly one of the particles in the loop in Fig. 3(a) must be heavy. Since the heavy masses do not vanish in the chiral limit, instead

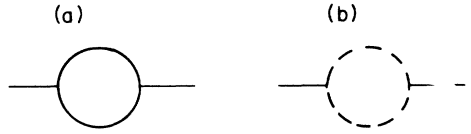

FIG. 3. More diagrams giving rise to chiral logarithms in m_π.

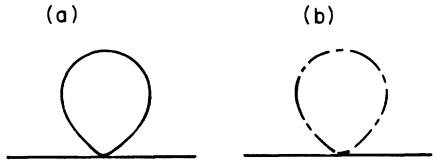

FIG. 4. More diagrams giving rise to chiral logarithms in m_π.

remaining of $O(1/a)$, the heavy propagators can be integrated out, leaving only diagrams of the form of Fig. 1(a). In practice, one simply does the calculation using the explicit form of the propagator G^π, which contains both heavy and Goldstone poles.

For $d=4$, the Figs. 2–4 give rise to leading-order chiral logarithms in m_π^2, as shown explicitly by Morel. That this is so is not surprising given the similarity of the graphs to that of Fig. 1(a). It should be mentioned that there are other corrections of order $1/d$ which modify the leading-order propagator, and thus shift the pion mass. These do not give rise to chiral logarithms, and will not be considered further.

In each of Figs. 2–4 there is a diagram with an internal pion, and a corresponding diagram with an internal fermion. The diagrammatic analysis predicts that there should be a complete cancellation between the diagrams of each pair. Morel's explicit calculation is in apparent contradiction with this claim. I have checked his calculation, and agree with his results. It turns out that while Figs. 2(a) and 2(b) do cancel, Figs. 3(a) and 3(b) do not, and neither do Figs. 4(a) and 4(b). Thus Morel finds a nonzero value for A_2^Q.

Having introduced the puzzle, I shall now explain its resolution. The key is to look at diagrams showing the constituent χ and ϕ fields of the mesons and fermions. For each of the diagrams in Figs. 2–4, there are a number of diagrams involving constituents. Representative examples are shown in Figs. 5–7, corresponding, respectively, to Figs. 2–4. The solid lines represent χ fields, the dashed lines ϕ fields. It may be useful to note that these constituent diagrams are precisely those that appear in a hopping-parameter expansion at strong coupling.[8]

First consider the tadpole diagrams of Fig. 5. Here Figs. 5(a) and 5(b) are contributions to Figs. 2(a) and 2(b), respectively. The important point is that there is a one-to-one correspondence between diagrams with internal χ

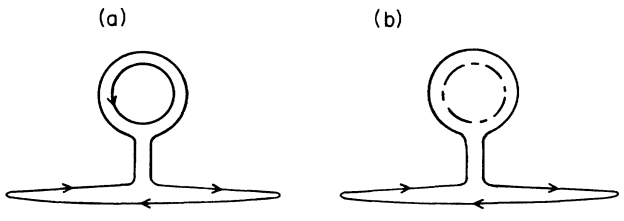

FIG. 5. Quark diagrams corresponding to the meson diagrams of Fig. 2. Solid lines are χ fields; dashed lines are ϕ fields.

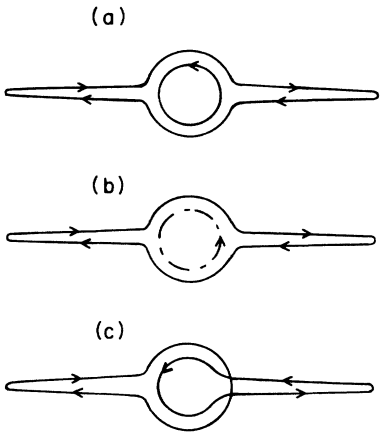

FIG. 6. Quark diagrams corresponding to the meson diagrams of Fig. 3.

and ϕ loops. Thus we would expect a complete cancellation between the diagrams, and this is what the calculations show.

In Fig. 6 however, there is an extra type of quark diagram contributing to the meson diagram of Fig. 3(a). This new type is illustrated by Fig. 6(c). The crucial point is that Fig. 6(c) does not contain an internal loop, unlike Figs. 6(a) and 6(b). Figure 6(c) differs from Fig. 6(a) only in the way that the quark lines are contracted together at the vertices. Thus they differ only by combinatoric factors. Because Fig. 6(c) does not contain an internal χ loop, it will not be canceled by diagrams with internal ϕ fields. On the other hand, one would expect Figs. 6(a) and 6(b) to cancel completely. This is indeed true, as shown in the next section. Thus the entire contribution from Fig. 3 comes from diagrams of the type shown in Fig. 6(c).

The new type of diagram thus explains why there can be chiral logarithms in Morel's calculation even in the quenched approximation. There is, however, another important feature of the diagram, namely, that it involves two disconnected quark lines. The χ field which begins at one of the pion sources ends *at the same source.* This means that such diagrams *are not included* in a standard quenched calculation of the pion propagator. In such calculations both quark and antiquark travel from one pion source to the other. Thus if one wants to compare to quenched pion calculations one must remove Fig. 6(c) by hand. Once this is done the loop diagrams cancel, and there are no chiral logarithms in quenched m_π.

An identical discussion applies to the diagrams of Fig. 7. There is an extra diagram, Fig. 7(c), which does not contain internal fermion loops, but which is disconnected. It is not present in the quenched pion propagator. Once it is excluded by hand, the remaining loop diagrams, Figs. 7(a) and 7(b), do cancel, and thus do not contribute chiral logarithms to m_π.

In summary, Morel's analysis correctly removes all contributions from internal fermion loops, but keeps some diagrams with disconnected quark lines. If the latter are removed by hand, then the loop diagrams cancel, and there are *no chiral logarithms* in quenched m_π. Since, as Morel demonstrates, there are also no chiral logarithms in the quenched condensate, the Gell-Mann–Oakes–Renner formula implies that there are also no chiral logarithms in quenched f_π. Thus the diagrammatic analysis is shown to be correct.

III. QUANTITATIVE CALCULATION

The mere existence of the diagrams shown in Figs. 6(c) and 7(c) suggests the resolution just described. To provide a technical justification, however, one must somehow separate the contributions of Figs. 6(a) and 6(c), and similarly Figs. 7(a) and 7(c). One way to do this is to introduce two species of staggered fermions: χ_1 and χ_2. If one considers the flavor-nonsinglet propagator

$$G_{xy}^{12,21}=\langle \bar{\chi}_1\chi_2(x)\bar{\chi}_2\chi_1(y)\rangle_C \ , \tag{6}$$

then the diagrams with disconnected quark lines [Figs. 6(c) and 7(c)] cannot contribute. Thus, if the discussion previous section is correct, the logarithms should cancel in this propagator in the quenched approximation. In fact, this nonsinglet propagator is precisely the pion propagator used in quenched calculations.

One can also pick out Figs. 6(c) and 7(c) by considering the off-diagonal propagator

$$G_{xy}^{11,22}=\langle \bar{\chi}_1\chi_1(x)\bar{\chi}_2\chi_2(y)\rangle_C \ . \tag{7}$$

This vanishes at leading order, but is nonzero at one loop. The discussion of the previous section predicts that the one-loop chiral logarithms should be identical to those for the quenched pion propagator for a single species of staggered fermion. Furthermore, the logarithms should be the same in quenched and unquenched calculations.

Finally one can calculate the diagonal propagator

$$G_{xy}^{11,11}=\langle \bar{\chi}_1\chi_1(x)\bar{\chi}_1\chi_1(y)\rangle_C \ . \tag{8}$$

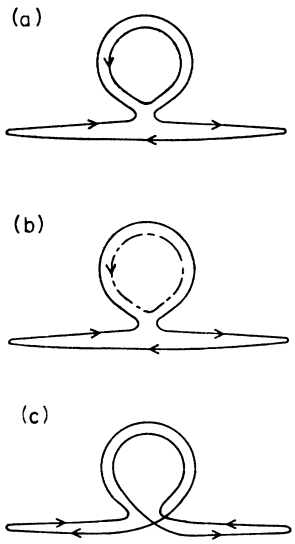

FIG. 7. Quark diagrams corresponding to the meson diagrams of Fig. 4.

In the quenched approximation the chiral logarithms in this propagator can only come from disconnected diagrams, and so should be identical to those in $G^{11,22}$. In the full theory, the logarithms should be given by the sum of those in $G^{12,21}$ (which come from internal loops) and those in $G^{11,22}$.

All these predictions of the diagrammatic analysis are borne out by the following calculation.

For the most part the calculation with two species (which I also call flavors) of staggered fermions is a simple extension of Morel's work. To define the quenched approximation one must introduce two scalar ghosts: ϕ_1 and ϕ_2. The partition function, in the strong-coupling limit, is then

$$Z_Q=\int\left[dU\prod_{i=1,2}d\chi_i d\bar{\chi}_i d\phi_i d\phi_i^\dagger\right]\times\exp\left[-S_1-S_2+\left[\frac{d}{2}\right]^{1.2}(j_{12}\bar{\chi}_2\chi_1+j_{21}\bar{\chi}_1\chi_2)\right]. \quad (9)$$

$$S_i=-\bar{\chi}_i\left[\not{D}_u+m_i+\left[\frac{d}{2}\right]^{1/2}j_{ii}\right]\chi_i+\phi_i^\dagger(\not{D}_U+\mu_i)\phi_i\ . \quad (10)$$

The gauge group is SU(N). Here and in the following, color indices, which are summed over, are implicit. The quenched approximation is obtained if $m_1=\mu_1$ and $m_2=\mu_2$. I have introduced four source terms to produce the four possible flavors of mesons. The propagators of interest can be obtained from the partition function as usual: for example,

$$G_{xy}^{12,21}=\frac{2}{d}\frac{\delta^2\ln Z_Q}{\delta j_{21}(x)\delta j_{12}(y)}\bigg|_{j=0}. \quad (11)$$

Integrating out the gauge fields and keeping only the leading term in a large-d expansion gives rise to an effective theory of composite mesons and fermions. For $N\geq 3$ the composite fields are

$$M_{ij}(x)=\frac{1}{N}\left[\frac{d}{2}\right]^{1/2}\bar{\chi}_i(x)\chi_j(x)\ , \quad (12)$$

$$H_{ij}(x)=\frac{1}{N}\left[\frac{d}{2}\right]^{1/2}\phi_i^\dagger(x)\phi_j(x)\ , \quad (13)$$

$$\bar{F}_{ij}(x)=\frac{1}{N}\left[\frac{d}{2}\right]^{1/2}\bar{\chi}_i(x)\phi_j(x)\ , \quad (14)$$

$$F_{ij}(x)=\frac{1}{N}\left[\frac{d}{2}\right]^{1/2}\phi_i^\dagger(x)\chi_j(x)\ . \quad (15)$$

For $N=2$ there are also baryonic composite fields. For the remainder of this section I will only consider $N\geq 3$.

It is convenient to group all fields, sources, and masses into flavor matrices: e.g.,

$$M=\begin{bmatrix}M_{11}&M_{12}\\M_{21}&M_{22}\end{bmatrix},\quad j=\begin{bmatrix}j_{11}&j_{12}\\j_{21}&j_{22}\end{bmatrix},\quad m=\begin{bmatrix}m_1&0\\0&m_2\end{bmatrix}. \quad (16)$$

The partition function of the effective theory which replaces Morel's I.8 can then be written (up to irrelevant overall factors)

$$Z_Q=\int[d\chi\,d\bar{\chi}\,d\phi\,d\phi^\dagger]e^{NS_{\rm eff}}\ , \quad (17)$$

$$S_{\rm eff}=-\sum_{x,y}\{\tfrac{1}{2}\mathrm{Tr}[M(x)V_{xy}M(y)]-\tfrac{1}{2}\mathrm{Tr}[H(x)V_{xy}H(y)]+\mathrm{Tr}[\bar{F}(x)V_{xy}F(y)]+\mathrm{Tr}[j(x)M(x)]+2\,\mathrm{Tr}(\bar{m}M)-2\,\mathrm{Tr}(\bar{\mu}H)\}\ , \quad (18)$$

where $\bar{m}=m(2d)^{-1/2}$, and $\bar{\mu}=\mu(2d)^{-1/2}$. The interaction matrix V connects nearest neighbors symmetrically; in momentum space it is

$$V=\frac{1}{d}\sum_\mu\cos q_\mu\ . \quad (19)$$

In Eq. (18) V is to be treated as proportional to the identity in flavor space.

One now introduces variables conjugate to the composite fields: λ, σ, Λ, and $\bar{\Lambda}$, respectively, for M, H, $\bar{F}$, and F. These conjugate variables are also 2×2 flavor matrices, defined exactly as in M in Eq. (16). Performing a Laplace transformation to make the action in Eq. (18) quadratic, doing the integration over the χ and ϕ fields, and shifting the variables λ and σ gives (up to an overall factor)

$$Z_Q=\int[d\lambda\,d\sigma\,d\Lambda\,d\bar{\Lambda}]\exp[-N(S_M+S_F)]\ , \quad (20)$$

where the mesonic and fermionic parts of the effective action are

$$S_M=\tfrac{1}{2}\mathrm{Tr}[(\lambda-2\bar{m}-j)V^{-1}(\lambda-2\bar{m}-j)]-\tfrac{1}{2}\mathrm{Tr}[(\sigma-2\bar{\mu})V^{-1}(\sigma-2\bar{\mu})]+\sum_x[-\mathrm{Tr}\ln\lambda(x)+\mathrm{Tr}\ln\sigma(x)]\ , \quad (21)$$

$$S_F=\mathrm{Tr}(\bar{\Lambda}V^{-1}\Lambda)+\sum_x\mathrm{Tr}\ln\left[1+\frac{1}{\sigma(x)}\bar{\Lambda}(x)\frac{1}{\lambda(x)}\Lambda(x)\right]. \quad (22)$$

The sum over the spatial indices of V^{-1} is implicit.

At this stage we have an interacting theory of composite mesons and fermions with a complicated, though local, polynomial interaction. In fact, when we are only interested in external composite bosons, as is true here, we can integrate out Λ and $\bar{\Lambda}$ analytically. This is possible because the Grassmann nature of Λ and $\bar{\Lambda}$ means that only the $\bar{\Lambda}\Lambda$ term in the expansion of the logarithm in Eq. (22) survives. The result is

$$Z_Q=\int[d\lambda\,d\sigma]\exp(-NS_M+S_\Lambda)\ , \quad (23)$$

in which the form of S_Λ is straightforward to compute, but lengthy to write. In the limit needed to compute the pion propagator S_Λ simplifies, and I will give the explicit form below. It contains vertices representing the loops of fermions appearing in Figs. 2(b), 3(b), and 4(b). In general these vertices are nonlocal, as in Fig. 3(b).

The final step in the calculation is to notice that the functional integral over λ and σ can be evaluated by expanding about the saddle point.[5] Correlation functions of λ and σ fields can then be written as a loop expansion in which each extra loop brings with it an extra power of $1/d$. The appearance of a nontrivial saddle indicates that chiral symmetry is broken.

As discussed by Morel, S_Λ should not be included in the calculation of the saddle, since it is a one-loop effect suppressed relative to S_M by $1/d$. Instead, the consistent procedure is to find the saddle of S_M, expand about it, and then add back in S_Λ. One should also set the source to zero when locating the saddle. Assuming that the fields are constant, and using $\sum_y V_{xy}^{-1}=1$, the saddle-point equations for λ reduce to

$$\lambda_{22}/\det\lambda=\lambda_{11}-2\bar{m}_1 , \tag{24}$$

$$\lambda_{11}/\det\lambda=\lambda_{22}-2\bar{m}_2 , \tag{25}$$

$$\lambda_{12}/\det\lambda=-\lambda_{21} , \tag{26}$$

$$\lambda_{21}/\det\lambda=-\lambda_{12} . \tag{27}$$

An identical set of equations, with $m\to\mu$, determine the saddle point for σ. For $\bar{m}_1\neq-\bar{m}_2$, as is true here, these equations require $\lambda_{12}=\lambda_{21}=0$, and also

$$1/\lambda_{11}=\lambda_{11}-2\bar{m}_1,\quad 1/\lambda_{22}=\lambda_{22}-2\bar{m}_2 . \tag{28}$$

These equations are both the same as that for a single species of fermion (see Morel I.17). At leading order in $1/d$, the two species of fermion do not interact. The solution to these equations, and the similar ones for σ, is

$$\lambda_{11}=\bar{\lambda}_1=\bar{m}_1+(\bar{m}_1^2+1)^{1/2} , \tag{29}$$

$$\sigma_{11}=\bar{\sigma}_1=\bar{\mu}_1+(\bar{\mu}_1^2+1)^{1/2} , \tag{30}$$

with similar equations for λ_{22} and σ_{22}. The choice of the positive root is explained by Morel.

The fields are now expanded about their saddle-point values. I will shift variables so that all fields vanish at the saddle, e.g., $\lambda_{11}\to\lambda_{11}-\bar{\lambda}_1$. One now does perturbation theory in the shifted fields. The propagators of interest are related to expectation values of λ fields. Applying the definition Eq. (11) to the partition function in Eq. (23) gives

$$G_{xy}^{12,21}\equiv -NV_{xy}^{-1}+N^2V_{xz}^{-1}\langle\lambda_{12}(z)\lambda_{21}(z')\rangle_C V_{z'y}^{-1} . \tag{31}$$

Similarly the other propagators are

$$G_{xy}^{11,11}=-NV_{xy}^{-1}+N^2V_{xz}^{-1}\langle\lambda_{11}(z)\lambda_{11}(z')\rangle_C V_{z'y}^{-1} , \tag{32}$$

$$G_{xy}^{11,22}=+N^2V_{xz}^{-1}\langle\lambda_{11}(z)\lambda_{22}(z')\rangle_C V_{z'y}^{-1} . \tag{33}$$

Here the connected λ two-point functions are to be evaluated using the partition function of Eq. (23), with $j=0$.

At leading order in $1/d$, we need only keep the tree diagrams. For these we must expand the action S_M to quadratic order in λ:

$$S_M=S_M(\bar{\lambda},\bar{\sigma})+\tfrac{1}{2}\mathrm{Tr}(\lambda V^{-1}\lambda)+\tfrac{1}{2}\mathrm{Tr}\left[\lambda\frac{1}{\bar{\lambda}}\lambda\frac{1}{\bar{\lambda}}\right]+O(\lambda^3) , \tag{34}$$

where $\bar{\lambda}=\mathrm{diag}(\bar{\lambda}_1,\bar{\lambda}_2)$. Expanding out the traces, one finds

$$\langle\lambda_{12}\lambda_{21}\rangle_C=\frac{\bar{\lambda}_1\bar{\lambda}_2}{N}\frac{V}{V+\bar{\lambda}_1\bar{\lambda}_2} , \tag{35}$$

$$\langle\lambda_{11}\lambda_{11}\rangle_C=\frac{\bar{\lambda}_1^2}{N}\frac{V}{V+\bar{\lambda}_1^2} , \tag{36}$$

$$\langle\lambda_{11}\lambda_{22}\rangle_C=0 . \tag{37}$$

So at leading order Eqs. (31) and (32) give

$$G^{12,21}\propto\frac{1}{V+\bar{\lambda}_1\bar{\lambda}_2},\quad G^{11,11}\propto\frac{1}{V+\bar{\lambda}_1^2} , \tag{38}$$

while $G^{11,22}$ vanishes. For $q=(\pi,\pi,\pi,\pi)+k$ these become

$$G^{12,21}\propto\frac{1}{k^2+2(\bar{m}_1+\bar{m}_2)d},\quad G^{11,11}\propto\frac{1}{k^2+4\bar{m}_1 d} , \tag{39}$$

showing the pseudo-Goldstone-boson pole with $m_{\pi(ij)}^2\propto m_i+m_j$.

As explained by Morel, the leading-order chiral logarithms come from one-loop contributions to the λ two-point functions. The diagrams which contribute are those shown in Figs. 2–4, except that the solid lines are now interpreted as λ propagators, and the dashed lines as Λ propagators. Let me first consider 2(a), 3(a), and 4(a), i.e., those diagrams not involving Λ loops. The propagators are given by Eqs. (35) and (36), and an analogous result for $\langle\lambda_{22}\lambda_{22}\rangle_C$. The required three- and four-point vertices are obtained by expanding the logarithm of λ in S_M [Eq. (21)]:

$$S_M^{(3)}=-\frac{1}{3}\left[\frac{\lambda_{11}^3}{\bar{\lambda}_1^3}+\frac{3\lambda_{11}\lambda_{12}\lambda_{21}}{\bar{\lambda}_1^2\bar{\lambda}_2}+(1\leftrightarrow2)\right] , \tag{40}$$

$$S_M^{(4)}=\frac{1}{4}\left[\frac{\lambda_{11}^4}{\bar{\lambda}_1^4}+\frac{4\lambda_{11}^2\lambda_{12}\lambda_{21}}{\bar{\lambda}_1^3\bar{\lambda}_2}+(1\leftrightarrow2)\right]+\frac{1}{4}\left[\frac{4\lambda_{11}\lambda_{22}\lambda_{12}\lambda_{21}}{\bar{\lambda}_1^2\bar{\lambda}_2^2}+\frac{2\lambda_{12}^2\lambda_{21}^2}{\bar{\lambda}_1^2\bar{\lambda}_2^2}\right] . \tag{41}$$

The calculation of Figs. 2(a), 3(a), and 4(a) is now completely straightforward. Including only these diagrams corresponds to the full, unquenched calculation. I give the results only for the flavor-symmetric limit:

$$\frac{N}{\bar{\lambda}^2}\langle\lambda_{12}\lambda_{21}\rangle_{C,UQ}=D_0+D_0\left[\frac{N_f}{N}\frac{2d_0}{1+\bar{\lambda}^2}+\frac{N_f}{N}D_0*D_0-\frac{2N_f}{N}d_0\right]D_0 , \tag{42}$$

$$\frac{N}{\bar{\lambda}^2}\langle\lambda_{11}\lambda_{11}\rangle_{C,UQ} = D_0 + D_0\left[\frac{N_f}{N}\frac{2d_0}{1+\bar{\lambda}^2} + \frac{N_f+1}{N}D_0 * D_0 - \frac{2N_f+1}{N}d_0\right]D_0 , \tag{43}$$

$$\frac{N}{\bar{\lambda}^2}\langle\lambda_{11}\lambda_{22}\rangle_{C,UQ} = D_0\left[\frac{1}{N}D_0 * D_0 - \frac{1}{N}d_0\right]D_0 , \tag{44}$$

where $N_f=2$. The terms on each line come, respectively, from the bare propagator, Figs. 2(a), 3(a), and 4(a). I have used Morel's notation:

$$D_0 = \frac{V}{V+\bar{\lambda}^2}, \quad d_0 = D_0(x,x) , \tag{45}$$

where here $\bar{\lambda}=\bar{\lambda}_1=\bar{\lambda}_2$ is no longer a flavor matrix. D_0 is proportional to the bare λ propagator, d_0 comes from the tadpole loops in Figs. 2(a) and 4(a). The notation $(D_0 * D_0)$ represents the loop integral in Fig. 3(a) (see I.36).

These results can now be plugged into Eqs. (31)–(33). The only point of importance here is that both d_0 and $(D_0 * D_0)$ contain chiral logarithms (see I.27 and I.40). Thus all three propagators contain chiral logarithms at the one-loop level in the full, unquenched theory. As discussed at the beginning of this section, the diagrammatic analysis predicts that the logarithms in $G^{12,21}$ should differ from those in $G^{11,11}$, because the former does not include contributions from disconnected diagrams such as Figs. 6(c) and 7(c). The contribution of these diagrams should be given by $G^{11,22}$. Thus one expects

$$\langle\lambda_{11}\lambda_{11}\rangle_C = \langle\lambda_{12}\lambda_{21}\rangle_C + \langle\lambda_{11}\lambda_{22}\rangle_C . \tag{46}$$

All these expectations are borne out by the results.

I have expressed the results in terms of N_f, the number of staggered species. The formulas have been derived only for $N_f=2$ but the N_f dependence can be deduced by seeing which diagrams contain internal fermion loops. In particular the result works also for $N_f=1$, the theory studied by Morel. The λ_{11} two-point function should be equal to Morel's result, and indeed Eq. (43) is identical to Morel's I.35 if $N_f=1$.

This completes the calculation in the full theory. For the quenched calculation one must add in the effect of the loops of Λ fields. These are represented by the action S_Λ, which is defined implicitly in Eq. (23). Since we are only interested in vertices involving λ, we can set $\sigma=\bar{\sigma}$. Then we have (up to an irrelevant constant)

$$S_\Lambda = \mathrm{Tr}\ln\left[V_{xy}^{-1} + \frac{1}{\bar{\sigma}_1}\delta_{xy}\frac{1}{\lambda}\right] + (1\leftrightarrow 2) . \tag{47}$$

The argument of the trace log is a matrix in the direct product of position space and flavor space. To evaluate Fig. 2(b) we need the term in S_Λ linear in λ_{ij} in an expansion about the saddle point. This is

$$S_\Lambda^{(1)} = -\frac{\lambda_{11}}{\bar{\lambda}_1}\left[\frac{V}{V+\bar{\lambda}_1\bar{\sigma}_1} + \frac{V}{V+\bar{\lambda}_1\bar{\sigma}_2}\right] + (1\leftrightarrow 2) . \tag{48}$$

In the flavor-symmetric limit, and with $\mu=m$, this reduces to

$$S_\Lambda^{(1)} = -N_f(\lambda_{11}+\lambda_{22})\frac{d_0}{\bar{\lambda}} , \tag{49}$$

For Figs. 3(b) and 4(b) we need the quadratic term in λ. Taking $\mu=m$, and going to the flavor-symmetric limit, this is

$$S_\Lambda^{(2)} = [\tfrac{1}{2}\lambda_{11}(x)\lambda_{11}(y) + \tfrac{1}{2}\lambda_{22}(x)\lambda_{22}(y) + \lambda_{12}(x)\lambda_{21}(y)]\left[\frac{2N_f d_0}{\bar{\lambda}^2}\delta_{xy} - \frac{N_f}{\bar{\lambda}^2}(D_0 * D_0)_{xy}\right] . \tag{50}$$

The first term in the large parentheses corresponds to the fermion loop in Fig. 4(b), since it is local in position space. The second term corresponds to the loop in Fig. 3(b).

It is straightforward to calculate Figs. 2(b), 3(b), and 4(b). One finds that Fig. 2(b) exactly cancels Fig. 2(a) in the λ_{11} and λ_{12} propagators. Similarly, Figs. 3(b) and 4(b) cancel Figs. 3(a) and 4(a), respectively, for the λ_{12} propagator. The final quenched results are

$$\frac{N}{\bar{\lambda}}\langle\lambda_{12}\lambda_{21}\rangle_{C,Q} = D_0 , \tag{51}$$

$$\frac{N}{\bar{\lambda}^2}\langle\lambda_{11}\lambda_{11}\rangle_{C,Q} = D_0 + D_0\left[\frac{1}{N}D_0 * D_0 - \frac{1}{N}d_0\right]D_0 , \tag{52}$$

$$\frac{N}{\bar{\lambda}^2}\langle\lambda_{11}\lambda_{22}\rangle_{C,Q} = D_0\left[\frac{1}{N}D_0 * D_0 - \frac{1}{N}d_0\right]D_0 . \tag{53}$$

As advertized, the loop diagrams, and the associated chiral logarithms, completely cancel from the nonsinglet pion propagator. The quenched result for the λ_{11} propagator is identical to that found by Morel (I.34). This is now understood as being due to the disconnected contributions, as shown explicitly by the equality of the corrections to $\langle\lambda_{11}\lambda_{11}\rangle_{C,Q}$ and $\langle\lambda_{11}\lambda_{22}\rangle_{C,Q}$.

IV. SU(2)

The calculation of Sec. III is not complete for SU(2), because there are baryonic composite fields such as $\epsilon_{\alpha\beta}\chi_\alpha\chi_\beta$, where the color indices are shown. There are also additional fermionic composites such as $\epsilon_{\alpha\beta}\phi_\alpha\chi_\beta$. These additional composite particles have Goldstone poles in their propagators, and so their loops can give rise to chiral logarithms.

Morel calculates the chiral logarithms in the condensate and in m_π for the single-flavor-SU(2) theory. The calculation for m_π suffers from the same problem as discussed previously, namely, the inclusion of contributions

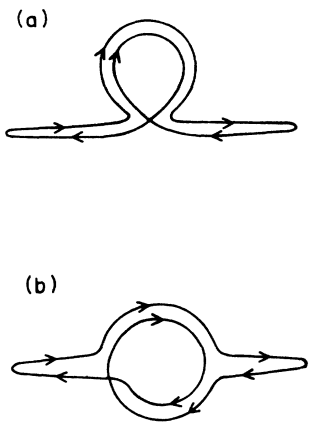

FIG. 8. Extra quark diagrams contributing chiral logarithms to m_π for SU(2) gauge theory.

from diagrams with disconnected quark lines. In fact this problem applies to both diagrams with mesonic $(\bar{\chi}\chi)$ and baryonic $(\chi\chi)$ loops. One might naively conclude, then, that if one excluded the disconnected diagrams by hand one would remove the chiral logarithms from m_π, just as for SU($N \geq 3$).

This conclusion is wrong, however, as pointed out to me by Morel.[9] There is, for SU(2), another type of diagram, in which the chiral logarithm comes from a Goldstone baryon loop, and which does not contain an internal fermion loop. Two examples for m_π are given in Fig. 8. These diagrams are connected, and so are present in the quenched pion propagator. Thus, even after removing the disconnected diagrams, the diagrammatic analysis predicts that there will be chiral logarithms in quenched m_π if the gauge group is SU(2).

I have not done the two-flavor-SU(2) calculation that is needed to extract the coefficient of the chiral logarithm. The quantitative value of the coefficient is not important. What is important is that the coefficient should not vanish, so that Morel's explanation of the numerical data obtained by Billoire and co-workers[2] remains tenable. I consider the diagrammatic analysis to be sufficiently justified by the results from Secs. II and III that another check is not crucial.

Morel's calculation of the chiral logarithms in the quenched condensate do, however, provide an indirect check on the diagrammatic analysis. For SU($N \geq 3$) the chiral logarithms in the quenched condensate are predicted to vanish by the diagrammatic analysis, and indeed do vanish in Morel's calculation. For SU(2), however, Morel shows that the quenched condensate has a nonvanishing chiral logarithm. The condensate is a one-point function, so there is no possibility that this result is due to disconnected quark diagrams, as for m_π. It can be understood, however, as being due to loops of Goldstone baryons coming from diagrams analogous to those in Fig. 8. So the diagrammatic analysis indeed predicts a chiral logarithm, as is found.

ACKNOWLEDGMENTS

I am very grateful to André Morel for pointing out to me that the results of Secs. II and III do not apply to SU(2), and for comments on the manuscript. I also thank Lowell Brown and Larry Yaffe for useful comments. This work was supported in part by the Department of Energy Outstanding Junior Investigator Program through Contract No. DE-AT06-88ER40423.

[1]A. Morel, J. Phys. (Paris) **48**, 1111 (1987).

[2]A. Billoire, R. Lacaze, E. Marinari, and A. Morel, Nucl. Phys. **B271**, 461 (1986).

[3]One might be worried by the fact that, because m_q is not a physical quantity, A depends on the renormalization scale. Similarly, the coefficients A_i are scale dependent. Does the whole discussion concern poorly defined quantities? This is not so, because in a lattice calculation the scale is determined by the inverse lattice spacing $1/a$, so A and the coefficients are well defined. Furthermore, one can phrase the issue of chiral logarithms in m_π entirely in terms of the ratio A_2/A_0: Does it vanish or not? This ratio is independent of scale.

[4]G. W. Kilcup, S. R. Sharpe, R. Gupta, and A. Patel, Phys. Rev. Lett. **64**, 25 (1990).

[5]H. Kluberg-Stern, A. Morel, and B. Petersson, Nucl. Phys. **B215**, 527 (1983); T. Jolicoeur, H. Kluberg-Stern, M. Lev, A. Morel, and B. Petersson, Nucl. Phys. **B235**, 455 (1984).

[6]G. W. Kilcup and S. R. Sharpe, Nucl. Phys. **B283**, 493 (1987).

[7]S. Sharpe (in preparation).

[8]O. Martin and A. Patel, Phys. Lett. B **174**, 94 (1986), and references therein.

[9]A. Morel (private communication).